Modulation of optical focusing by using optimized zone plate structures

Jia-Han Li,* Chih-Hong Lin, Yao-Jen Tsai, Yi-Wei Cheng, and Tony Wen-Hann Sheu

Department of Engineering Science and Ocean Engineering, National Taiwan University, No. 1, Sec. 4, Roosevelt Road, Taipei 10617, Taiwan

**jiahan@ntu.edu.tw*

Abstract: The focusing properties of the optimized zone plate structures which have upper and lower zones with different thicknesses are studied by the three-dimensional finite-difference time-domain method. Two kinds of materials are chosen, including silver representing metal and BK7 glass representing dielectric. An optimization algorithm is applied to tune the parameters of zone plate structures. Several optimized zone plate structures with smaller circular-shape focus are presented. By using the angular spectrum representation method, we found that the cases with smaller focal sizes have larger high-*k* components; however, the intensities of side lobes also become larger in comparison with the main beam. It is also found that the phase differences between different spatial field components can have the influences on focusing properties. A special case with two focuses is shown by changing the cost function of the same optimization algorithm. Our findings suggest that the optimized zone plate structures can reconstruct the light intensity distribution and have a great potential for the applications in imaging, lithography, and data storage.

OCIS codes: (240.6680) Surface plasmons; (050.1965) Diffractive lenses; (050.1970) Diffractive optics.

References and links

1. Y. Fu, W. Zhou, L. E. N. Lim, C. L. Du, and X. G. Luo, "Plasmonic microzone plate: Superfocusing at visible regime," Appl. Phys. Lett. **91**(6), 061124 (2007).
2. Y. Fu, and W. Zhou, "Modulation of main lobe for superfocusing using subwavelength metallic heterostructures," Plasmonics **4**(2), 141–146 (2009).
3. Y. Fu, Y. Liu, X. Zhou, Z. Xu, and F. Fang, "Experimental investigation of superfocusing of plasmonic lens with chirped circular nanoslits," Opt. Express **18**(4), 3438–3443 (2010).
4. A. G. Curto, A. Manjavacas, and F. J. García de Abajo, "Near-field focusing with optical phase antennas," Opt. Express **17**(20), 17801–17811 (2009).
5. H. C. Kim, H. Ko, and M. Cheng, "Optical focusing of plasmonic Fresnel zone plate-based metallic structure covered with a dielectric layer," J. Vac. Sci. Technol. B **26**(6), 2197–2203 (2008).
6. H. C. Kim, H. Ko, and M. Cheng, "High efficient optical focusing of a zone plate composed of metal/dielectric multilayer," Opt. Express **17**(5), 3078–3083 (2009).
7. Q. Wang, X. Yuan, P. Tan, and D. Zhang, "Phase modulation of surface plasmon polaritons by surface relief dielectric structures," Opt. Express **16**(23), 19271–19276 (2008).
8. J. Li, Y. Cheng, Y. Chue, C. Lin, and T. W. Sheu, "The influence of propagating and evanescent waves on the focusing properties of zone plate structures," Opt. Express **17**(21), 18462–18468 (2009).
9. R. G. Mote, S. F. Yu, B. K. Ng, W. Zhou, and S. P. Lau, "Near-field focusing properties of zone plates in visible regime - New insights," Opt. Express **16**(13), 9554–9564 (2008).
10. R. Merlin, "Radiationless electromagnetic interference: Evanescent-field interference lenses and perfect focusing," Science **317**(5840), 927–929 (2007).
11. A. Grbic, L. Jiang, and R. Merlin, "Near-field plates: Subdiffraction focusing with patterned surfaces," Science **320**(5875), 511–513 (2008).
12. A. Grbic, and R. Merlin, "Near-field focusing plates and their design," IEEE Trans. Antenn. Propag. **56**(10), 3159–3165 (2008).
13. R. Gordon, "Proposal for superfocusing at visible wavelengths using radiationless interference of a plasmonic array," Phys. Rev. Lett. **102**(20), 207402 (2009).
14. L. E. Helseth, "The almost perfect lens and focusing of evanescent waves," Opt. Commun. **281**(8), 1981–1985 (2008).

#132228 - $15.00 USD Received 23 Jul 2010; revised 17 Sep 2010; accepted 6 Oct 2010; published 13 Oct 2010

15. L. E. Helseth, "Radiationless electromagnetic interference shaping of evanescent cylindrical vector waves," Phys. Rev. A **78**(1), 013819 (2008).
16. M. Perez-Molina, L. Carretero, P. Acebal, and S. Blaya, "Optical singularities and power flux in the near-field region of planar evanescent-field superlenses," J. Opt. Soc. Am. A **25**(11), 2865–2874 (2008).
17. F. M. Huang, and N. I. Zheludev, "Super-resolution without evanescent waves," Nano Lett. **9**(3), 1249–1254 (2009).
18. F. L. Pedrotti, S. J. and L. S. Pedrotti, *Introduction to Optics* (Prentice-Hall International, 2nd ed., 1993), Chap. 18.
19. E. D. Palik, *Handbook of Optical Constants of Solids* (Academic Press, San Diego, 1985).
20. X. He, J. Wu, X. Li, X. Gao, L. Zhao, and L. Wu, "Synthesis and properties of silicon dioxide films prepared by pulsed laser deposition using ceramic SiO2 target," Appl. Surf. Sci. **256**(1), 231–234 (2009).
21. L. Novotny, and B. Hecht, *Principles of Nano-Optics* (Cambridge University Press, 2006), Chap. 2.

1. Introduction

The Fresnel zone plate structures are widely used as the focusing lenses in optical applications, such as microscopy, imaging, lithography, etc. Recent studies in plasmonic zone plate structures show that better focusing properties can be achieved. For example, the zone plate structures with metal and dielectric material have a highly-directional focal beam with the focal size smaller than the diffraction limit in the visible wavelength region [1–3] or infrared light region [4]. The zone structure covered with the other dielectric layer [5] or metal-dielectric multilayer [6] is found to have a better focus. The phase of surface plasmon polaritons can be modified by varying the dielectric structure on a metal surface, and an in-phase phase modulation Fresnel zone plate is proposed to either enhance or suppress the field intensity [7]. By analyzing the fields in the focal plane, larger high-k components are seen in the k-domain for the silver zone plates than for the glass zone plates, and the smaller focus can be obtained for the silver zone plates [8]. The focuses of different metal coated Fresnel zone plate structures in the visible range are smaller than the diffraction limit because the evanescent field affects the near field focusing [9]. A higher resolution can be obtained by the radiationless electromagnetic interference [10–13]. The contribution of the evanescent waves to the total electromagnetic field behind the subwavelength apertures has been studied [14,15]. Also, the Poynting flux in these structures was found to have optical singularities in the near field region [16]. Without the help of evanescent waves, a superoscillating focusing design with only propagating waves was proposed in [17]. These findings show that the plasmonic zone plate structures with specific geometries and materials can reconstruct the light intensity distribution and have a great potential in nanophotonic applications.

In this paper, we assume the zone plate structures with the upper zones and lower zones which may have the same or different materials. We use an optimization algorithm to tune the zone thicknesses and study the field in the focal plane by the finite-different time-domain method. Several optimized structures are obtained and analyzed by the angular spectrum representation. The focusing properties of these optimized zone plate structures are studied and their physical mechanisms are described. One special case with two focuses is also demonstrated by modifying the cost function used in the same optimization procedures.

2. Zone plate structures and simulation setup

A standard Fresnel zone plate having the same thickness of each zone can be used to focus the plane wave. We use an optimization procedure by tuning the thickness of the zones to find better focusing properties. Figure 1 shows the cartoon of the zone plate structure under current study. The upper zones and lower zones with the same radius have different thickness. The transparent zones are air and the dark zones are silver or BK7 glass. The radius of the zones can be calculated by the equation $R_n = ((d + n\lambda_0/2)^2 - d^2)^{1/2}$ [18], where R_n is the radius of n_{th} zone, n is the number of the zone, d is the focal distance, and λ_0 is the wavelength of the incident light. We assume that the radius of the outermost zone, which looks like the substrate, is infinite.

We apply the three-dimensional finite-difference time-domain method to study the focal properties of zone plate structures. The mesh is a cubic with the length 10 nm. The perfectly matched layers are applied at the outer boundaries to simulate the infinite space. We consider

#132228 - $15.00 USD Received 23 Jul 2010; revised 17 Sep 2010; accepted 6 Oct 2010; published 13 Oct 2010

the incident light with x polarization and wavelength 632.8 nm. The focal plane is at z = 1 μm. The dielectric constants of the silver and BK7 glass can be found in [19,20].

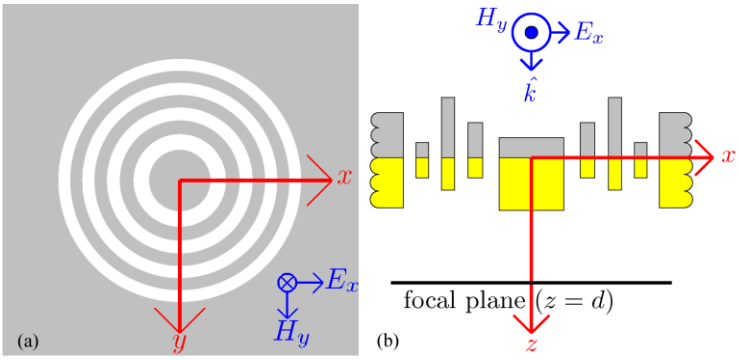

Fig. 1. A cartoon of the investigated zone plate structure with different thickness in each zone, where (a) is the top view and (b) is the cross view.

3. Optimization algorithm and optimized structures

By tuning the parameters and the materials of the zone plate structures, the size, shape and distance of focus change accordingly. The focusing properties can be evaluated by the full width half maximum (FWHM) of the focal size in the focal plane. The focus with a smaller focal size and circular shape are preferred. If there are N parameters and M steps in total for each parameter, there are M^N possibilities of different structures. For example, the 4-air-zone structure with different thickness of upper and lower zones shown in Fig. 1 has 27^{10} possibilities of the structures if the zone thickness varies for every 20 nm from 20 nm to 540 nm. This demands a huge amount of computational time if the simulations for all structures need to be done. Thus, it is required to have an algorithm or the procedure to find the optimized zone plate structures. Here, we propose an optimization algorithm and describe the procedures in below to find the optimized zone plate structures with smaller focus.

The optimization method we use can be represented in terms of a cost function which is defined as the focal size in the focal plane that depends on the zone plate structures. For the sake of ease, we only change the thickness of each zone and fix the zone radius and focal plane at z = 1 μm during the optimization procedures. We consider the cost function

$$c(t_u, t_l) = f_x + f_y \tag{1}$$

with the following two limiting conditions

$$\left| f_x - f_y \right| < w_1 \times \max(f_x, f_y) \tag{2}$$

and

$$\max(P_z(x, y \notin f, z = 1\mu m)) < w_2 \times \max(P_z(x, y \in f, z = 1\mu m)), \tag{3}$$

where t_u and t_l are the thicknesses of the upper zones and lower zones from the inner zone to the outer zone, f_x and f_y are the FWHMs of focus along x and y directions in the focal plane at z = 1 μm, f is the focal region, w_1 is the coefficient relating to the focus shape, w_2 is the coefficient relating to the ratio of the intensities of the side lobes and main beam, and $P_z(x, y, z = 1\ \mu\text{m})$ is the z-component of the average power density normalized by the incident plane wave in the focal plane at z = 1 μm. The P_z can be expressed by the following equation

$$P_z = (\frac{1}{2}\text{Re}(E_x \times H_y^* - E_y \times H_x^*)) / (\frac{1}{2}\text{Re}(E_{ix} \times H_{iy}^*)), \tag{4}$$

#132228 - $15.00 USD Received 23 Jul 2010; revised 17 Sep 2010; accepted 6 Oct 2010; published 13 Oct 2010

where E and H are the electric field and magnetic field, respectively, * denotes complex conjugate, and Re(·) means taking the real part of · , E_i and H_i are the electric field and magnetic field of the incident plane wave, respectively, the subscript x or y means the x or y component of the field. In Eq. (2), w_1 is in the range of 0 and 1. If w_1 is smaller, the focus turns out to be more circular. If w_1 is larger, the focus turns out to be more elliptical. In Eq. (3), if w_2 is smaller, the ratio of the intensities of side lobes and main beam becomes smaller. If w_2 is in the range of 0 and 1, the main beam is on the focal region. Otherwise, the main beam is in the region outside of the focal region. In this paper, we assume $w_1 = 0.1$ for a more circular shape and $w_2 = 0.5$ for the intensities of the side lobes being smaller than half of the main beam. Thus, the optimization procedure is to minimize the cost function with the limiting conditions by tuning the zone thickness and varying the zone plate structures. In the first step, we have to choose a structure as the initial structure which has the small value of the cost function in Eq. (1) and satisfies the two limiting conditions in Eqs. (2) and (3). The standard structure with fixed thickness for each zone is one of the candidates as being the first structure, or we can choose one structure with random thickness of each zone from all possibilities and simulate their focusing properties by finite-difference time-domain method. If the structure has the small value of cost function as shown in Eq. (1) and satisfies two limiting conditions as shown in Eqs. (2) and (3), it is chosen as the initial structure during the optimization procedures. In our experiences, it needs to take at least ten structures to find one structure as the candidate of the initial structure. In the following steps, we randomly choose one zone and vary its thickness to yield a thinner or thicker zone. If the cost function does not get smaller or the focusing properties do not satisfy the two limiting conditions, the original value of the chosen zone thickness keeps unchanged. If the cost function gets smaller and the focusing properties satisfy the two limiting conditions, we continue to vary this chosen zone to a thinner or thicker zone until the value of the cost function cannot get smaller or the focusing properties do not satisfy the two limiting conditions. The value of the newly chosen zone thickness is used in the next step. Then, we randomly choose the other zone and repeat these procedures by checking their cost function values and two limiting conditions. We repeat these procedures until the cost function value is not changed or changed only by a negligibly small value with satisfying the two limiting conditions.

We use the proposed optimization algorithm for the zone plate structures with five zones. The structure parameters of the optimized designs and their focusing properties are shown in Table 1, and the standard zone plate is also listed in Table 1 for comparison. The material of the upper and lower zones for cases 1 to 3 is silver. In case 1, we fix the lower zone thickness t_l and tune the upper zone thickness t_u. In case 2, we fix t_u and tune t_l. In case 3, we tune t_u and t_l both. In case 4, the material of upper zones is silver and the material of lower zones is BK7 glass, and both t_u and t_l are tuned. For case 1, the initial structure is a random structure as t_u = {20, 500, 60, 140, 20} and t_l = {20, 20, 20, 20, 20}. For case 2, the initial structure is also a random structure as t_u = {20, 20, 20, 20, 20} and t_l = {300, 20, 140, 180, 100}. Because the cases 3 and 4 have double parameters as comparing to the cases 1 and 2, we choose the standard zone plate structure with fixed zone thickness t_u = {40, 40, 40, 40, 40} and t_l = {0, 0, 0, 0, 0} as the initial structure for cases 3 and 4 to avoid the difficulty to search for one initial random structure. Figure 2 shows the cost function values verse the number of simulation for these cases by using the proposed optimization algorithm. The optimized structures for all cases can be found within one hundred times of FDTD simulations. Our FDTD simulations are done in the computer with Intel Xeon E5520 Nehalem 2.26GHz Quad-Core CPU and 24 GB DDR-3 1333MHz memory. If only one core of Quad-Core CPU is used, the average computation time for one FDTD simulation with the mesh size 10 nm cubic and the whole simulation domain is 12 μm × 12 μm × 3.6 μm in this computing resource needs about 150 minutes. If all cores in CPU or parallel computing are used, the computation time can be much reduced. This shows that the optimized zone plate structures can be obtained in the reasonable computational time by our proposed optimization procedures.

#132228 - $15.00 USD Received 23 Jul 2010; revised 17 Sep 2010; accepted 6 Oct 2010; published 13 Oct 2010

Table 1. The zone thicknesses (t_u and t_l), FWHMs (f_x and f_y), the maximum of z-component of average power density normalized by the incident plane wave (max. P_z), and the focal size for the standard zone plate structure and the optimized structures

	t_u (nm)	t_l (nm)	f_x (nm)	f_y (nm)	*max.* P_z	focal size (nm^2)
standard	20, 20, 20, 20, 20	0, 0, 0, 0, 0	269.8	269.9	15.3	5.71*10^4
case 1	0, 520, 200, 40, 140	20, 20, 20, 20, 20	242.1	255.8	5.1	4.86*10^4
case 2	20, 20, 20, 20, 20	440, 100, 40, 20, 20	245.2	235.7	3.0	4.54*10^4
case 3	20, 160, 20, 20, 140	440, 20, 40, 20, 0	245.5	229.8	2.3	4.43*10^4
case 4	380, 520, 160, 40, 80	440, 20, 0, 0, 40	242.9	241.5	3.9	4.60*10^4

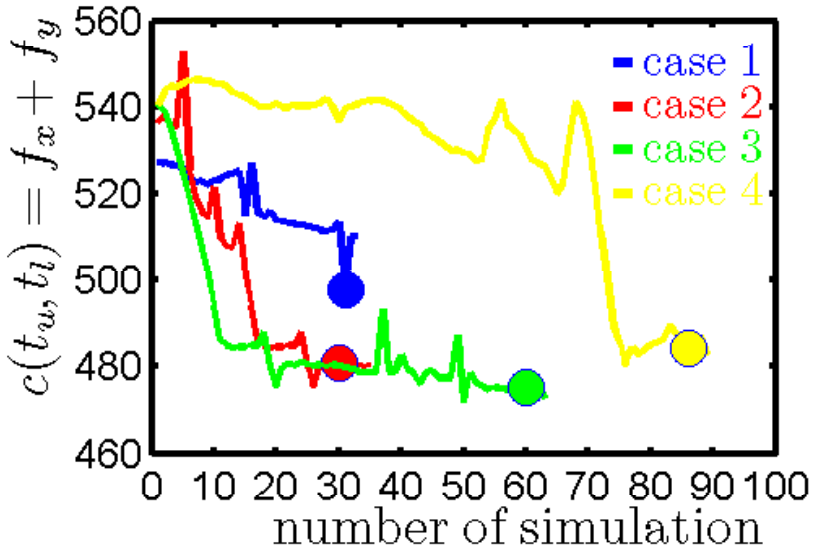

Fig. 2. The cost function values $c(t_u, t_l) = f_x + f_y$ verse the number of simulation during the proposed optimization procedures. The circles are the final optimized zone plate structures.

4. Results and discussion

Figure 3 shows $P_z(x, y)$, the average power density normalized by the incident plane wave in the focal plane at $z = 1$ μm, in space domain for all cases in Table 1, and their focal sizes can be estimated by the contours of half intensities of the focuses being shown as the white dashed lines in Fig. 3(b), 3(d), 3(f), 3(h), and 3(j). The focal size of each case is also listed in Table 1. For example, the focal size of case 4 is about 4.6*10^4 nm^2 which is similar to the standard zone plate with 25 air zones.

To understand the focusing properties of the standard and optimized cases, Fig. 4 shows the normalized z-component of the average power density divided by its maximum along x and y directions in space domain in the focal plane of all cases in Fig. 3 or listed in Table 1. The results show that the optimized structures have smaller sizes and smaller intensities in focus than the standard zone plate structure. Although the focal sizes of the optimized cases are smaller than the standard case, the side lobes get larger and the shapes of some focuses for optimized cases are not circular as the standard case.

#132228 - $15.00 USD Received 23 Jul 2010; revised 17 Sep 2010; accepted 6 Oct 2010; published 13 Oct 2010

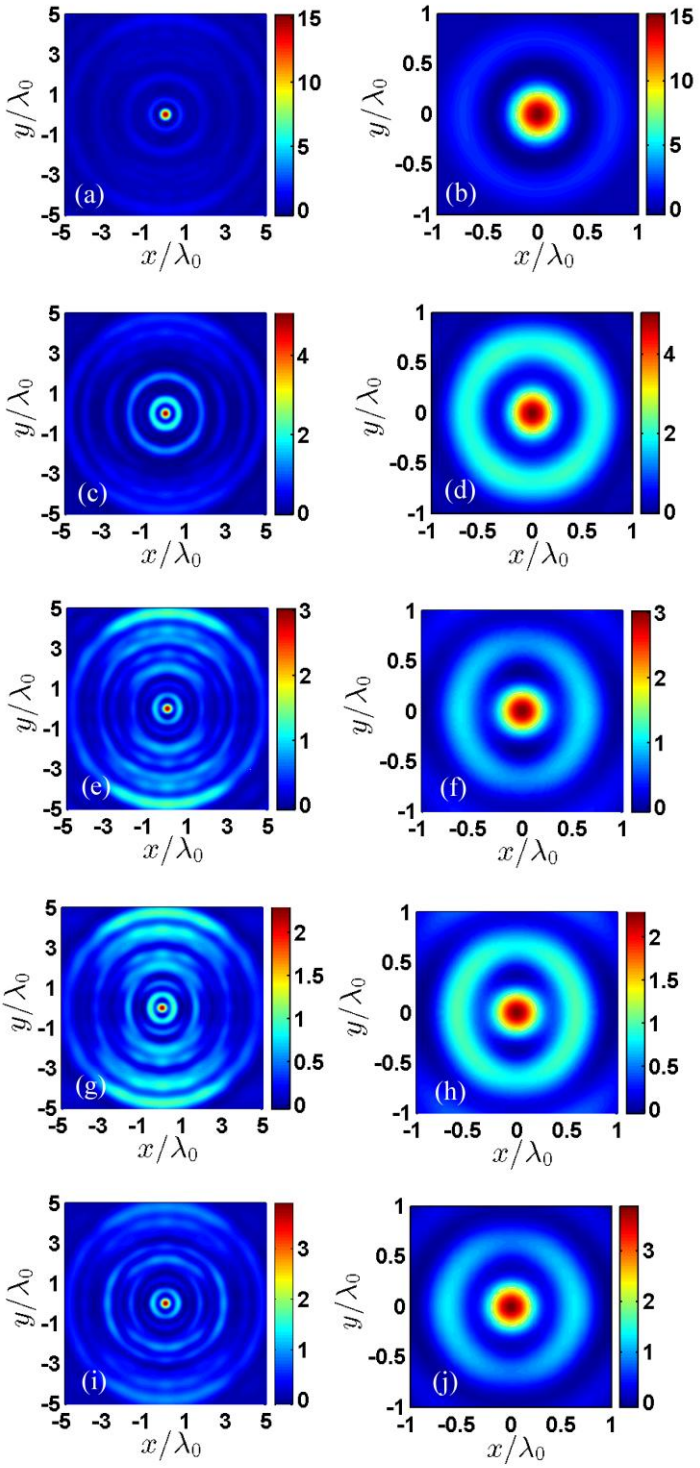

Fig. 3. (a), (c), (e), (g), and (i) are the simulated $P_z(x, y)$ for the cases standard, 1, 2, 3, and 4 in Table 1, and (b), (d), (f), (h), (j) are the zoom-in plots of (a), (c), (e), (g), and (i) where the white dashed lines are the contours of half intensity of the focus.

#132228 - $15.00 USD Received 23 Jul 2010; revised 17 Sep 2010; accepted 6 Oct 2010; published 13 Oct 2010

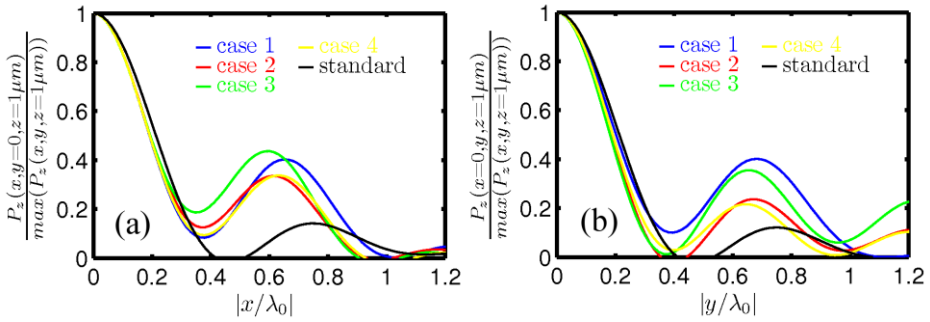

Fig. 4. The simulated normalized $P_z(x, y)$ divided by its maximum along the lines of (a) $y = 0$ and (b) $x = 0$ in the focal planes ($z = 1$ μm) for the cases tabulated in Table 1.

By using the angular spectrum representation [21], the field in the *k*-domain in a specific plane can be calculated by taking the Fourier transform of the field in the space domain for the same plane. When observing the field in the *k*-domain for the focal plane, we know the intensities of the fields with different k_x and k_y in the focal plane. The field in the range of $k_x^2 + k_y^2 < k_0^2$ is the propagating wave with the propagating constant $k_z = (k_0^2 - k_x^2 - k_y^2)^{1/2}$. The field in the range of $k_x^2 + k_y^2 > k_0^2$ is the evanescent wave with an attenuation constant $\alpha_z = (k_x^2 + k_y^2 - k_0^2)^{1/2}$. Figure 5 shows the normalized *z*-component of the average power density divided by its maximum along k_x and k_y directions in the *k*-domain in the focal plane of all cases in Table 1. Comparing to Fig. 4 and Fig. 5, the cases with smaller focal sizes have larger high-*k* components and side lobes. The components of the field in the *k*-domain can be varied by tuning the thickness and material of zone plate structures, and the field in space domain changes accordingly. In the investigated cases, we found that the side lobes get larger as the focal size becomes smaller during the optimization procedures.

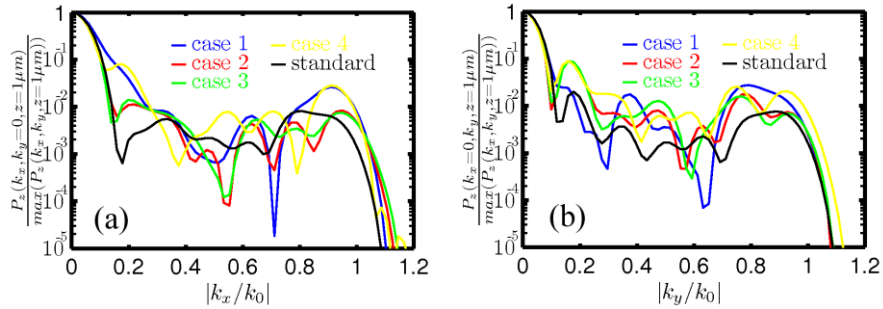

Fig. 5. The simulated normalized $P_z(k_x, k_y)$ divided by its maximum along the lines of (a) $k_y = 0$ and (b) $k_x = 0$ in the focal planes ($z = 1$ μm) for the cases tabulated in Table 1.

From the *k*-domain analysis results in Fig. 5, the spatial field component around $0 \le |k_x| \le 0.1k_0$ or $0 \le |k_y| \le 0.1k_0$ is much strong because the incident wave is the plane wave which has the spatial field component $k_x^2 + k_y^2 = 0$ and diffracts from the zone plate structures. There are other spatial field components which have peaks around $0.2k_0 \le |k_x| \le 1.1k_0$ or $0.2k_0 \le |k_y| \le 1.1k_0$ in Fig. 5. These peaks are related to the air rings in the zone plate structure as shown in Fig. 1. Because the thickness of each zone is different for the optimized cases, the light propagating from each zone as shown in Fig. 1 to the focus in the focal plane can not be all in phase. To understand the influences of phase difference on the focusing properties, we can use the angular spectrum representation again. We can assume that there are specific spatial field components in the *k*-domain and transfer to the field in the space domain by taking the inverse Fourier transform of the spatial field in the *k*-domain. To avoid the

#132228 - $15.00 USD Received 23 Jul 2010; revised 17 Sep 2010; accepted 6 Oct 2010; published 13 Oct 2010

complexity as shown in Fig. 5, we take the combination of the spatial field components which include $0 \le k_x^2 + k_y^2 \le (0.1k_0)^2$, $(0.2k_0)^2 \le k_x^2 + k_y^2 \le (0.3k_0)^2$, $(0.4k_0)^2 \le k_x^2 + k_y^2 \le (0.5k_0)^2$, $(0.6k_0)^2 \le k_x^2 + k_y^2 \le (0.7k_0)^2$, and $(0.8k_0)^2 \le k_x^2 + k_y^2 \le (1.1k_0)^2$. Assuming all spatial field components are in phase and the intensities of the component $0 \le k_x^2 + k_y^2 \le (0.1k_0)^2$ are ten times larger than other components, its transformed space field as the blue line shown in Fig. 6 can be obtained by taking the inverse Fourier transform from all spatial field components. Keeping the phase of the component $0 \le k_x^2 + k_y^2 \le (0.1k_0)^2$ unchanged and varying only the phase of all other field components for case 1, the results with the phase differences $\frac{\pi}{4}$, $\frac{\pi}{2}$, and $\frac{3\pi}{4}$ between the value of $0 \le k_x^2 + k_y^2 \le (0.1k_0)^2$ and other spatial field components are shown as cases 2, 3, and 4, respectively, in Fig. 6. It is interesting to find that the results of the cases 2, 3, and 4 in Fig. 6 have smaller focal sizes but larger side lobes. This is similar as the results for optimized cases in Fig. 4. To study the influence of the other spatial field components, the case 5 in Fig. 6 shows the intensities of all other components double the intensities except $0 \le k_x^2 + k_y^2 \le (0.1k_0)^2$ as comparing to the conditions in case 1. It shows that this case can also give better focus but larger side lobes. If we only double the intensity of the component $(0.8k_0)^2 \le k_x^2 + k_y^2 \le (1.1k_0)^2$ as comparing to the conditions in case 1, the case 6 in Fig. 6 shows better focus but also larger side lobes than case 1 and case 5. For the in-phase cases 1, 5, and 6 in Fig. 6, we found that the first and the other minimums for these cases are zero. For the non-in-phase cases 2, 3, and 4 in Fig. 6, the first and the other minimums for these cases are not zero. This is a very important information because similar phenomena are also observed for the optimized zone plate structures in Fig. 4.

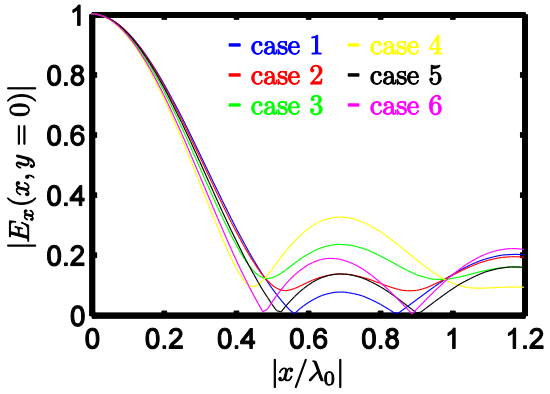

Fig. 6. The predicted values of the normalized $|E_x(x, y = 0)|$ along the line y = 0 for different combinations of the field components in the k-domain. The field in case 1 (blue line) is all in phase: 10 ten-time intensity of $0 \le k_x^2 + k_y^2 \le (0.1k_0)^2$ with one-time intensity of other components including $(0.2k_0)^2 \le k_x^2 + k_y^2 \le (0.3k_0)^2$, $(0.4k_0)^2 \le k_x^2 + k_y^2 \le (0.5k_0)^2$, $(0.6k_0)^2 \le k_x^2 + k_y^2 \le (0.7k_0)^2$, and $(0.8k_0)^2 \le k_x^2 + k_y^2 \le (1.1k_0)^2$. The case 2 (red line), case 3 (green line) and case 4 (yellow line): there are phase differences $\frac{\pi}{4}$, $\frac{\pi}{2}$, and $\frac{3\pi}{4}$ between $0 \le k_x^2 + k_y^2 \le (0.1k_0)^2$ and other spatial field components, respectively. The case 5 (black line): the intensities of all other components double the intensities except $0 \le k_x^2 + k_y^2 \le (0.1k_0)^2$ as comparing to the conditions in case 1. The case 6 (magenta line): the intensity of the component $(0.8k_0)^2 \le k_x^2 + k_y^2 \le (1.1k_0)^2$ doubles the intensity as comparing to the conditions in case 1.

#132228 - $15.00 USD Received 23 Jul 2010; revised 17 Sep 2010; accepted 6 Oct 2010; published 13 Oct 2010

Combining the discussion of influences of phase and the intensities of high-*k* and evanescent waves, the focusing properties of the optimized zone plate structures have a better physical explanation. Thus, the focusing properties of a structure can be modified by varying the parameters of the structure and controlling the phase effect and the field distribution in the *k*-domain.

Modifying the cost function Eq. (1) to $c(t_u, t_l) = f_x$ and removing the limitations of Eqs. (2) and (3) in the optimization procedures and keeping the other conditions unchanged, a structure with silver upper zones t_u = {40, 40, 40, 380, 540} and BK7 glass lower zones t_l = {420, 60, 100, 20, 400} is found to have two focuses in its centric of the focal plane. The *z*-component of the average power density normalized by the incident plane wave for this structure is shown in Fig. 7(a), and Fig. 7(b) is the zoom-in plot of Fig. 7(a). The focal size of each focus can be estimated by the contours of half intensity of the focus, which is shown as the white dashed lines in Fig. 7(b). The focal size is about $1.2*10^5$ nm^2. The distance of two focuses shown as the cross marks in Fig. 7(b) is about 800 nm. It should be noticed that the intensities of the side lobes in Fig. 7(a) are larger than the intensities of the two focuses in the centric of the focal plane because of the removal of the two imposed limitations in Eqs. (2) and (3).

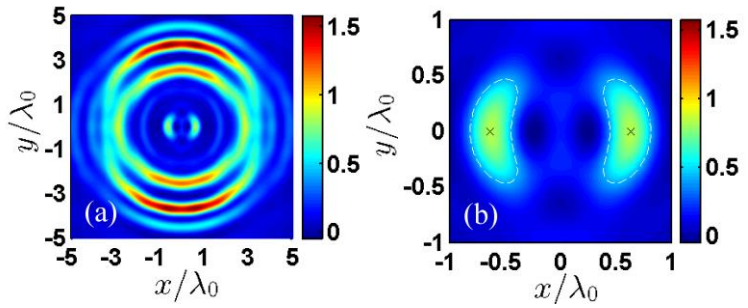

Fig. 7. Two-focus case: (a) The simulated $P_z(x, y)$ which is normalized to the incident plane wave, and (b) is the zoom-in plot of (a) where the white dashed lines are the contours of half intensity of the focuses.

5. Conclusions

Based on the finite-difference time-domain method and the proposed optimization algorithm, several optimized plasmonic zone plate structures are found to have better focusing properties with smaller focal sizes and acceptable side lobe intensities. From the angular spectrum representation method, the smaller focus can be generated and has larger high-*k* components in the *k*-domain; however, the intensities of the side lobes also get larger. The focusing properties are influenced by the phase differences between different spatial field components. We also present another two-focus design by changing the cost function and removing the limitation conditions in the optimization procedures. These studies show that the functional optical structures can be designed solely by varying the thicknesses of the zone plate structures, and it is expected that a better performance can be achieved if more parameters are considered in the optimization procedures, such as the material, zone radius, etc.

Acknowledgments

This work was supported by the National Science Council, Taiwan (NSC-96-2221-E-002-133-MY3, NSC-98-2120-M-002-004, NSC-98-2120-M-009-007, NSC-98-2221-E-002-164-MY3), and the National Taiwan University Innovative Research Funds (NTU-98R0333). We are grateful to the National Center for High-Performance Computing, Taiwan, for providing us the requested computer time and facilities.